



Dynamic modelling of methanol steam reforming to hydrogen in a packed bed reactor for shipboard fuel cells

Bojan Grenko^a,^{*}, Wiebren de Jong^b, Robert van de Ketterij^c, Lindert van Biert^a

^a Maritime Transport and Technology Department, Delft University of Technology, Mekelweg 2, Delft, 2628 CD, The Netherlands

^b Process and Energy Department, Delft University of Technology, Leeghwaterstraat 39, Delft, 2628 CB, The Netherlands

^c Military Technological Sciences Department, Netherlands Defence Academy, Het Nieuwe Diep 8, Den Helder, 1781 AC, The Netherlands

ARTICLE INFO

Keywords:

Methanol steam reforming
Forced operation
Unsteady 2D model
Maritime

ABSTRACT

Hydrogen economy is spreading across the maritime sector in response to increasingly stringent regulations for shipping emissions. The challenging on-board hydrogen logistics are often mitigated with hydrogen carriers such as methanol. Research on methanol reforming to hydrogen for fuel cell feed is conducted mostly in steady state, overlooking dynamic reactor operation and its effects on the power production system. Forced reactor operations induce fluctuations of CO content in the reformat potentially harmful to the PEM fuel cell, and drops in methanol conversion causing inefficient operation. In present research, simulations with a physical 2D unsteady model of a packed bed methanol steam reforming reactor resulted in methanol conversion drop durations of up to a minute. Additionally, temporary increases of CO content up to 112% were observed. Throughput ramp ups most notably impact the conversion, while ramp downs negatively affect selectivity. The investigation on reactor geometry concludes that larger tube diameters increase transient time and CO spikes, while they decrease with reactor length. Amplified unsteady effects are also observed with larger changes in input process variables. The results imply that heat transfer rate to the reactor are most often the detrimental factor for transient effects and durations in practice. Following this work, inclusion of realistic heating methods is recommended, instead of uniform tube temperatures used in present simulations. Heating system characteristics are necessary for realistic evaluation of the methanol reformer constraint on fuel cell feed demand in fully integrated systems.

1. Introduction

The maritime sector faces increasing reduction requirements for airborne emissions [1–3]. Compliance with these restrictions motivates the sector towards fuel cell technology, which is inherently more compliant to the emission requirements. Proton exchange membrane fuel cells (PEMFC) namely are a mature and high power density solution [4,5], but require pure hydrogen as fuel to function effectively. However, the gravimetric density of hydrogen storage systems are low and limiting for maritime [6], and these bunkering solutions scale up poorly [7,8].

Methanol is currently one of the most attractive hydrogen carriers for the maritime sector due to its liquid state at standard conditions, availability, scale-up potential, and relatively simple on-site reforming process to produce hydrogen [9–12]. Furthermore, methanol can be produced renewably from captured CO₂ and green electricity based H₂ [13], making it more likely to be a part of lasting solution. On-board methanol reforming to hydrogen become more advantageous with

higher requirements of ship range, speed, and endurance. In such cases, the fuel then becomes the dominant component in the energy system size and weight [4], and the benefits of fuel energy density outweigh the addition of the reforming system. The first practical application of this concept was in 2023 with Hydrogen One towboat [14], which validated its viability and demonstrated the potential for other ships.

In transport applications, dynamic power requirements introduce additional obstacles, particularly within the methanol reformer. Two significant and interconnected added considerations are response time in forced operation, and reformer lifetime. First, the forced operation in catalytic processes causes fluctuations in product composition [15]. Stable composition and fast reactor transient time are conflicting objectives, adding a layer of complexity in comparison to steady operation. Second, dynamic operation is expected to affect the system lifetime [15,16]. The forced reactor operation causes fluctuations in internal temperature field which potentially accelerates catalyst sintering.

^{*} Corresponding author.

E-mail address: b.grenko@tudelft.nl (B. Grenko).

<https://doi.org/10.1016/j.cej.2025.160623>

Received 1 November 2024; Received in revised form 5 February 2025; Accepted 12 February 2025

Available online 20 February 2025

1385-8947/© 2025 The Authors. Published by Elsevier B.V. This is an open access article under the CC BY license (<http://creativecommons.org/licenses/by/4.0/>).

Furthermore, the fluctuating levels of produced CO could damage the fuel cell if they are not expected and separated prior to it.

The CO content in the reformer product is problematic because CO rapidly deactivates the PEMFC anode catalyst. Low temperature PEMFC manufacturers often specify CO limits at 0.2 ppm according to standard ISO 14687-2 [17–19], which commercial methanol reformers achieve with Palladium membranes for hydrogen separation [20,21]. The size and energy requirement of the separation process depends on the expected amounts of CO [22]. Predictions of CO content fluctuations are thus important for separation process sizing, and prevention of PEMFC poisoning during forced operation.

This work investigates a tubular packed bed methanol steam reforming reactor in unsteady operation using a 2D model. Present simulations consider transient aspects the reformer, such as internal temperature field and reformat composition. Unsteady analyses are innately left out of most research on methanol reforming, since the field predominantly focuses on novel conceptual systems and integration in steady state operation [23–26]. The aim of this study is to indicate reformer transient time between two steady states through methanol conversion and CO fluctuation in the product, and reflect on their impact for integration with PEM fuel cells. These outcomes define additional operating constraints of methanol steam reformer and contribute to inputs for design of methanol reforming based maritime power system.

2D physics based model using finite difference approach was used to conduct simulation cases of four transient events on four reactor geometries. The effects of differences in forced operation inputs and reactor dimensions are shown, and analysed for their impact on transient time and produced CO fluctuations. Finally, the simulated reactor behaviour is contextualized against model simplifications, reformer integration with PEMFC, specific reactor heating methods.

2. Background and scope

This section provides the context of the investigated configurations of the methanol reformer, significant process variables, and the selection process of simulation boundary conditions.

2.1. Background

2.1.1. Methanol reforming reactor

Methanol reformer coupling with PEMFC most commonly utilize methanol steam reforming [11,23,24,26,27]. This endothermic steam reforming process has highest hydrogen production and selectivity among the reforming methods [28]. Methanol steam reforming (MSR) reaction equations are (i) methanol steam reforming:



(ii) the water-gas shift (WGS):



and (iii) methanol decomposition (MD):



Methanol reformer configuration is most commonly a multitube packed bed reactor filled with copper-zinc based catalyst pellets. This arrangement, as shown in Fig. 1, is at present time the most commercially attainable arrangement [23,29,30]. First, the copper-zinc based catalysts are non-expensive, most active for MSR, and highly selective towards hydrogen [31]. Second, the tube-in-shell heat exchanger with multiple packed beds is a robust arrangement suitable for various heating fluids. This design is also easily scalable, and fitting for hydrogen throughput and reactor sizes required for large power consumers in a maritime setting.

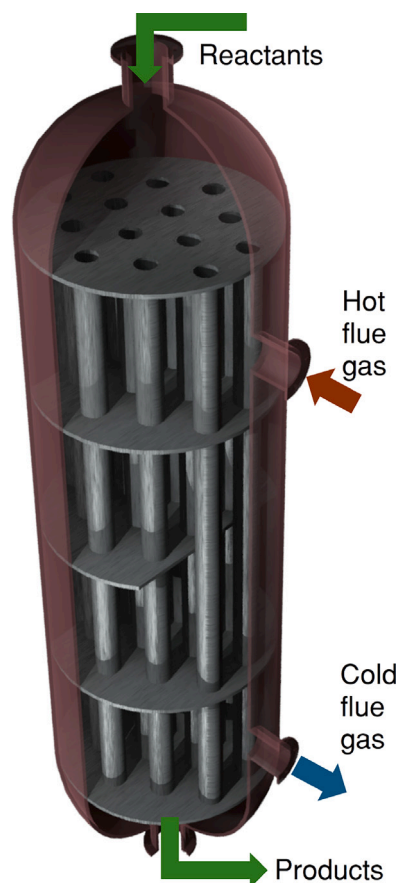


Fig. 1. Tube-in-shell reactor heated with flue gas.

2.1.2. Reformer operation characteristics

The transient time of methanol reformer, which is the time required for change between two steady operational states, is a significant characteristic since it propagates through the entire power production system. Transients dictate the size, weight, and overall necessity for hydrogen buffer tanks and/or batteries required for peak shaving. The PEM fuel cell has a transient response within seconds [32–34]. On the other hand, transient times in reforming systems are unknown, and commercial systems manufacturers only indicate startup from hot standby duration within the range of 5–45 min [29,30,35], depending on the unit size and requested H_2 flow rate. Reformer transient time could likely be a transient characteristic of the entire power system.

Dynamic loads are specific to every ship, and therefore the required transient capabilities of a methanol reformer vary as well. Generally, the reformer does not necessarily need to be as fast as PEMFC in load changes, as long as the ship operation is not limited. A reference point for required transient capabilities is found in comparisons with marine internal combustion engines (ICE). Specifications of ICE manufacturers indicate 1–6 min for 100% load ramp up, mainly dependant on the engine temperature [36,37]. If the reformer transient times are comparable to those of ICEs, similarity can also be expected in the total size and weight of peak shaving components.

Another important aspect of reformer transients is their effect on hydrogen separation strategy. Reformat composition fluctuates during forced reactor operation, and deviates from values expected for intermediate steady states [15]. Large deviations potentially cause lower H_2 recovery and resulting H_2 purity with the chosen method [38,39]. It is crucial that all CO in particular is removed from the reformat, since it is extremely poisonous to the low temperature PEMFC anode. Such poisoning from repeated dynamic operations is cumulative, and

the extent of this problem is unknown. Hydrogen separation methods are not directly studied in present work, and instead the CO amount is quantified as expected input value to the separation process.

2.1.3. Alternative MSR reactor heating methods

Apart from flue gas, heat exchangers can also use other heating media. Liquid media such as heat transfer oil have higher density and heat capacity, ensuring lower axial temperature, lower velocity, and higher heat transfer coefficient on the shell side [40,41]. By using steam as a heating medium, the reaction heat can be supplied through latent heat of condensation. The shell side temperature becomes relatively constant, and is set through the shell side pressure. Moreover, the heat transfer coefficient is higher than in heating with flue gas [40]. The possibility of using listed heating media is beneficial in design flexibility, and integration with other potentially present thermodynamic cycles. By using the same working fluid and a centralized heating system for multiple shipboard processes, higher efficiency and better space utilization can be obtained.

The overall goal of carbon emission reductions is diminished if reactor heat is provided through combustion. Electrified heating for steam reforming is one potential answer to clean heat supply, fitting for electrification of ships. Their advantages include compactness due to absence of heating fluid and furnaces, reduced heat transfer limitations, and direct heating control. However this technology is still in development. Kim, Lee, and Lee [42] note the majority of research is on the laboratory scale, and recommend optimization of reactor materials, and integrated studies with renewable energy technologies such as solar or fuel cells. Idamakanti et al. [43] report issues with catalyst stability in electrified catalyst reactors. While the electrified technology is promising, more research is required prior to commercial use.

2.2. Scope and assumptions

The present study aims to provide an indication of characteristic methanol reformer transient times through numerical modelling, and how they are influenced by parameters such as reactor size and input process variables. The assumptions of this study stem from chosen model fidelity, explored geometric parameters, and simulated heating method, which are described in this subsection. The findings intend to demonstrate a reliable framework for predicting unsteady methanol steam reforming operations.

2.2.1. Reactor model fidelity

Simulations are conducted on a single packed bed tube within a fixed multitube reactor. The focus of the present work is on the changing internal process variable fields, such as heat transfer and reaction rates, as well as the effects of unsteady developing interactions within the flow field. The differences between individual tubes are disregarded, assuming that provided heating is equal across the whole reactor.

The reference model for present work is the 2D steady state model of Zhu et al. [44,45], experimentally validated in a lab scale packed bed reactor filled with cylindrical catalyst particles, using gas analysers on the reformer outlet stream. This model is fitting for present investigations due to its fidelity level and low computational cost. The model is able to capture radial heat transfer and its interaction with internal 2D reformer fields. Simultaneously, the computational effort is not wasted on high fidelity level, as the simulations can run effectively on local machines. The alternative of fully comprehensive CFD models result in a highly detailed flow fields, but make parametric studies impractical due to the necessity for high performance computing [46,47]. The steady state model equations of Zhu et al. are:

$$u_s \frac{\partial C_i}{\partial z} = D_{er} \left(\frac{\partial^2 C_i}{\partial r^2} + \frac{1}{r} \frac{\partial C_i}{\partial r} \right) + \eta_i \rho_c r_i, \quad (4)$$

$$u_s \rho_f c_{p,f} \frac{\partial T}{\partial z} = \lambda_{er} \left(\frac{\partial^2 T}{\partial r^2} + \frac{1}{r} \frac{\partial T}{\partial r} \right) + \sum \eta_j \rho_c (-\Delta H_j) r_j S_c, \quad (5)$$

where ε is the porosity, C_i (mol m⁻³) are the species concentrations, u_s (m s⁻¹) is the flow superficial velocity, D_{er} (m² s⁻¹) is the effective radial mass diffusion coefficient, ρ_c is the catalyst bulk density, r_i is the production rate of component i , T (K) is the temperature, λ_{er} (W m⁻¹ K⁻¹) is the effective radial thermal conductivity, ΔH (J mol⁻¹) is the reaction heat, r_j is the reaction rate of reaction j , S_c (m⁻² kg⁻¹) is the catalyst surface area, and η are the effectiveness factors. Additionally, the Ergun equation [48] is used to calculate pressure field in the bed. The kinetics model for CuO/ZnO/Al₂O₃ of Peppley et al. [49] is used, which is based on a Langmuir-Hinshelwood mechanism for surface reactions. This kinetic model includes all the three reversible dominant reactions of MSR (Eq. (1)–(3)). Detailed model description and formulae of all terms can be found in the comprehensive work of Zhu et al. [44,45,50].

2.2.2. Geometric parameter influence

Reactor tube dimensions influence the internal heat transfer, which affects reaction rates and consequently the composition of fuel cell feed. Heat transfer was identified as the dominant limiting mechanism of methanol steam reforming by Yoon et al. [51] in their experimental study. The two currently relevant ways of influencing the heat transfer are varying (i) the reactor tube diameter, and (ii) flow velocity. Reducing the internal diameter d_i decreases maximum radial heat penetration depth, and the increases ratio of heated area to internal volume. The flow velocity, however, affects heat transfer indirectly via radial mass transport. The internal radial mixing has a positive correlation with the superficial velocity u_s , which is reflected through the effective radial diffusion coefficient D_{er} and the effective radial thermal conductivity λ_{er} in model Eqs. (4)–(5). Lengthening a reactor while keeping diameter d_i and residence time t_{res} constant therefore improves the internal heat transfer. Reactor diameter and length are therefore varied for capturing heat transfer differences in steady and dynamic operation.

2.2.3. Simulated reactor heating

A uniform axial wall temperature profile is used for all simulated cases in present work. In reality, the axial heat profile is specific to a heating method, which is defined during reactor design through parameters such as energy efficiency, complexity, control, reactor size, and other system objectives. Compactness and energy efficiency are valued in maritime applications, so potential for integration with waste heat from other sub-systems is likely an influencing factor for on-board reactors. Analysis of heating methods extends the study towards system differences, while the objective of current work is internal reactor dynamics. A theoretical uniform wall temperature profile is used limit the study, and minimize differences in heating boundary conditions.

Reactor wall temperature in dynamic simulations changes according to step functions. Despite not being realistic, a step function represents the most drastic change in wall temperature, highlights reactor natural response. The realistic gradual changes impose their own transient time, obscuring the natural response of the reactor caused by its catalyst thermal capacity. Furthermore, a realistic wall heating transient time is caused by circumstances such as heating method and control strategy, which are not a part of this study. Consequently, a step function in this context is a straightforward and the most meaningful comparison of different reformer tube geometries.

3. Methods

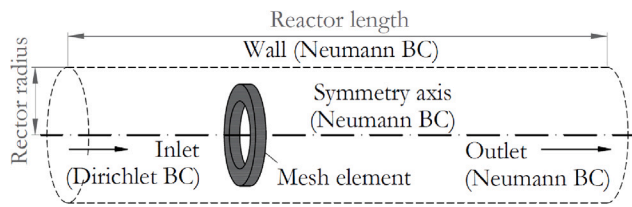
3.1. Dynamic model description

Dynamic model was created by extending original Zhu's model with the temporal term and heat capacities. The new equations of mass and energy balances are:

$$\varepsilon \frac{\partial C_i}{\partial t} = -u_s \frac{\partial C_i}{\partial z} + D_{er} \left(\frac{\partial^2 C_i}{\partial r^2} + \frac{1}{r} \frac{\partial C_i}{\partial r} \right) + \eta_i \rho_c r_i, \quad (6)$$

Table 1
Simulation boundary conditions.

	Coordinates	Boundary condition
Inlet	$z = 0$	$C_i = C_0$
	$0 \leq r \leq r_{max}$	$T = T_0$
Outlet	$z = z_{max}$	$\frac{\partial C_i}{\partial z} = 0$
	$0 \leq r \leq r_{max}$	$\frac{\partial T}{\partial z} = 0$
Wall	$0 \leq z \leq z_{max}$	$\frac{\partial C_i}{\partial r} = 0$
	$r = r_{max}$	$\frac{\partial T}{\partial r} = -\frac{U_i}{\lambda_{er}}(T_{wall} - T)$
Symmetry axis	$0 \leq z \leq z_{max}$	$\frac{\partial C_i}{\partial r} = 0$
	$r = 0$	$\frac{\partial T}{\partial r} = 0$

**Fig. 2.** Reactor single tube computational domain and boundary condition (BC) types.

$$\begin{aligned}
 &(\epsilon \rho_f c_{p,f} + (1 + \epsilon) \rho_s c_{p,s}) \frac{\partial T}{\partial t} = \\
 &-u_s \rho_f c_{p,f} \frac{\partial T}{\partial z} + \lambda_{er} \left(\frac{\partial^2 T}{\partial r^2} + \frac{1}{r} \frac{\partial T}{\partial r} \right) \\
 &+ \sum \eta_j \rho_c (-\Delta H_j) r_j S_c.
 \end{aligned} \quad (7)$$

The unsteady equations in this work are not validated against experimental data. However, the unsteady terms add interactions between heat storage capacities of catalyst and gas, which are well known material properties. The model is hence expectedly reasonably accurate for unsteady predictions.

The used in-house solver [52] is implemented in Python®. All unsteady cases were simulated on a local machine with Intel i7 processor within 30 min computation time. A finite difference approach is used on a uniform mesh with element size of $5e-3$ m. The axial derivatives of species concentrations C_i and temperature T are evaluated with a 2nd order upwind scheme, while the radial derivatives are evaluated with a 4th order central difference scheme. Time is discretized with 4th order Runge–Kutta scheme, with time step size of $1e-4$ s. The fitting time step and grid size was determined with sensitivity analyses to ensure that fast reaction rates were properly captured, which simultaneously resulted in a Courant number below $8.5e-3$. The simulation boundary conditions are given in Table 1, and a graphical representation of the computational domain is shown in Fig. 2.

3.2. Simulation cases

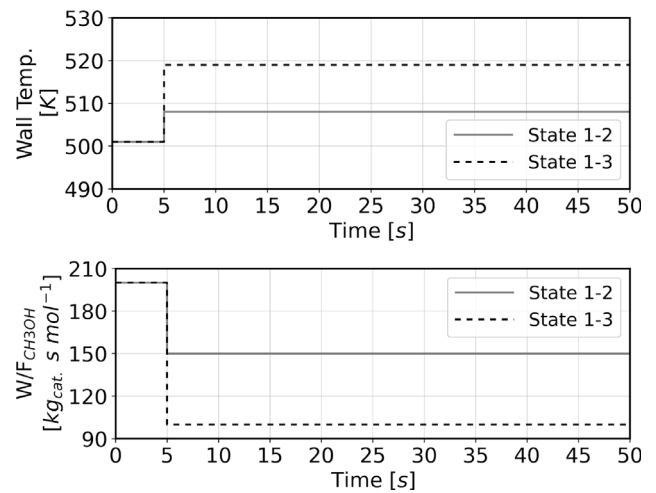
Simulations are performed on four reactor geometries, whose exact dimensions are presented in Table 2. The tube diameters are chosen in accordance with experimental work in the literature [51,53–55], where 20 and 30 mm diameters are common for a MSR reactor. Diameters in this range are shown to effectively transfer heat radially in steady state, so they were chosen to extend the analysis to unsteady operation. Reactor lengths in present study are defined through aspect ratios (AR), or length-to-width ratios. Thus superficial velocity, and effective radial mixing remain comparable across diameter changes. In experimental studies [51,53–55] the reactors are often relatively small, with aspect ratios ranging between 20 and 50. On industrial scale, comparable reactors are found in methane steam reforming where aspect ratios range between 60 and 130 [56]. In present work, aspect ratios of 25

Table 2
Dimensions of four simulated reactor geometries.

Reactor label	Internal diameter d_i [mm]	Reactor length l [mm]	Aspect ratio AR (l/d_i) [-]
d20 AR25	20	500	25
d20 AR100	20	2000	100
d30 AR25	30	750	25
d30 AR100	30	3000	100

Table 3
Process variables of simulated steady states.

Steady state	W_{cat}/F_{CH_3OH} [kg s mol ⁻¹]	T_{wall} [K]	Feed increase in ref. to state 1
1	200	501	0%
2	150	508	50%
3	100	519	100%

**Fig. 3.** Dynamic boundary conditions of T_{wall} (top) and W_{cat}/F_{CH_3OH} (bottom) for increasing H_2 production according to states presented in Table 3.

and 100 were chosen as representations of experimental and industrial reactor lengths. All simulations are performed assuming a commercial MSR catalyst with mass composition 40% CuO, 40% ZnO, and Al₂O₃ to balance. Catalyst pellets are spherical in shape with a diameter of 1.5 mm.

The transient reactor behaviour is observed by showcasing step changes between pre-defined steady states. The process variables of these steady states are chosen by first picking the representative values of methanol feed, W_{cat}/F_{CH_3OH} (kg s mol⁻¹), with respect to literature [50,51,53–55]. The methanol feed is defined with respect to catalyst mass to make the performance comparisons valid across different scales. The wall temperature, T_{wall} , was then calculated with a simple 1D isothermal model. The calculations targeted a methanol conversion of $X_{CH_3OH} = 95\%$ at the reformer outlet, under 3 bar pressure and inlet feed temperature of 523 K. Conversion below 100% is intentionally targeted in the simulation steady states so that conversion increases in transient events may also be captured. The resulting feed and reactor wall temperatures of three steady states, named 1–3, correspond to the three reactor throughputs, and are given in Table 3.

Four dynamic events are simulated for each of the reactor geometries. Boundary condition step functions of T_{wall} and W_{cat}/F_{CH_3OH} are shown in Figs. 3 and 4. The four events represent step changes between three steady states described in Table 3: small throughput increase (state 1–2), large throughput increase (state 1–3), small throughput decrease (state 2–1), and large throughput decrease (state 3–1). State 1 is the reference steady state in all simulations, where states 2 and

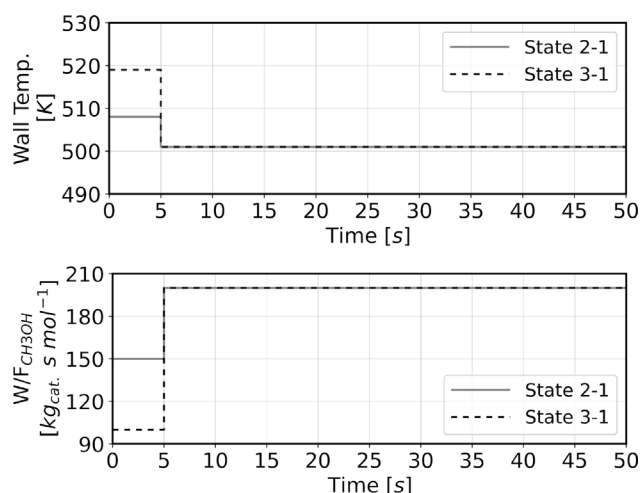


Fig. 4. Dynamic boundary conditions of T_{wall} (top) and W_{cat}/F_{CH_3OH} (bottom) for decreasing H_2 production according to states presented in Table 3.

3 represent throughput changes by 50% and 100%, respectively. Step functions for input process variables are used to emphasize changes in reactor internal flow field variables, and to ensure the results are not influenced by realistic supporting equipment such as feed pump or reactor heater.

4. Results

4.1. Steady state results and dimension effects

Conversion in 2D simulations is expected to deviate from the targeted 95%, due to different radial mixing and heat transfer rates specific for each geometry. These effects can be seen in Fig. 5, which shows internal temperature field plots of all four geometries at steady state 1. The difference between all simulated geometries and steady states are shown in the supplementary material in Figures A.1 – A.3. All cases display a cold spot near the inlet caused as the highest methanol concentration within the reactor, which is likely unavoidable. The relative size of the inlet cold spot grows with higher diameter and lower aspect ratio. These differences in the internal temperature distribution affect the conversion and product composition in both steady and transient operation, as shown in the next subsection (see Fig. 6).

4.2. Dynamic simulation results

The results in this section predominantly show the reactor responses to large step function inputs, which shift between steady state 1–3, and state 3–1. The results presented in main text most clearly illustrate the performance trends, while full results are provided in the supplementary material in Figure A.4.

The results in Figure 6 consist of three plots: CH_3OH conversion, CO content in dry product gas, and relative H_2 rate. The CH_3OH conversion most evidently shows the reactor transient time. It corresponds to stabilization of the disturbed internal temperature field. Tracking CO content in the dry product gas is directly linked to H_2 selectivity, due to the WGS reaction changing its direction after all methanol in the reactor has been consumed. Furthermore, this plot shows the amount of CO, and magnitude of its fluctuations in transients, indicating the varying amount of CO that must be separated before reaching the PEMFC. Finally, relative hydrogen production in time is shown. The H_2 rate at the outlet is shown relative to ideal steady state conversion of the reactant feed, previously defined as 95% conversion. This plot highlights the delay and deviation between required and

Table 4

Comparison of reactor geometry influence on performance characteristics during H_2 production 100% ramp up (state 1–3), and ramp down to the original state (state 3–1).

Reactor	Time for CH_3OH conv. to reach within 5% of new value during ramp up [s]	Max. increase of CO in dry product during ramp down
d20-AR25	30	95%
d30-AR25	57 ^a	112%
d20-AR100	11	42%
d30-AR100	23	68%

^a Outside of plotted range in Fig. 6(b)

produced H_2 rate. All plots are shown on a 50 s timeline. In this time, the plotted variables reach 97% of the values for new steady states, with the exception of d20-AR25 reactor whose variables react slowly and approach around 90% of the new steady state.

The CH_3OH conversion displays two distinct trends for ramp up, and ramp down events. In ramp ups, the conversion in all cases drops for approximately two seconds before reaching the local minimum, indicating how the reaction draws heat from the catalyst. The time for conversion to increase again varies among reactors and depends on geometric factors since the added heat penetrates the reactor radially, while the methanol feed $W_{cat}F_{CH_3OH}$ is in immediate flow contact with the entire catalyst mass. Larger diameters hence take longer to entirely heat up to new steady state. Longer reactors however have a quicker response, since the constant residence time causes higher velocity which promotes internal mixing and radial heat transfer. The positive geometric influences are seen on the AR100 reactors which reach new steady state the fastest, with the d20-AR100 showing the lowest relative drop in conversion. The opposite is seen on d30-AR25, which does not reach equilibrium within 50 s.

In the ramp down events, the conversion temporarily spikes up, caused by thermal heat storage capacity of the catalyst, since it holds excessive heat for the new steady state. However, the magnitude of conversion disturbance is lower than in the ramp up event. The heat consumption by the reactants works in favour of achieving the equilibrium with lower average internal temperature, and the geometry has a lesser impact than in ramp ups. This is further supported by Fig. 7, which shows CH_3OH conversion for all dynamic events on one reactor. Overall, the ramp down events show highly similar and uniform conversion trends, with low influence from the geometry.

The CO drop during ramp ups can be linked to the drop in conversion and overall lower reaction rates due to internal temperature decrease. In ramp downs, the spike up is caused by the reverse water gas shift reaction, which continues to produce CO at maximum conversions due to the thermal energy contained in the catalyst. The CO oscillation magnitude in simulated cases is linked to reactor volume and the amount of catalyst. The oscillation magnitude can be decreased with gradual temperature changes, allowing the catalyst temperature to progressively adapt. This signifies an additional check for reactors in transient operation, especially in large scale reactors operating at conversions close to 100%.

Finally, the achieved H_2 production rate plots show high correlation to CH_3OH conversion plots. The longer reactors show more pronounced production dips and spikes, but also stabilize quicker afterwards. Most notably, the d30-AR100 reactor produces similar relative H_2 rates as d20-AR100 despite having lower conversion, indicating higher selectivity towards hydrogen. Since these reactors have same AR, the selectivity increase is possibly caused by better radial mixing due to higher velocity. This is supported by temperature field plot in Fig. 5 which shows lower average temperature in d30-AR100, causing lower rate of reverse WGS reaction and better H_2 selectivity.

The influence of reactor geometry is quantified in Table 4 for H_2 ramp up from steady state 1 to state 3, and subsequent ramp down back to state 1. Comparisons in ramp ups are evaluated with time needed for the reactor to reach 95% conversion value of the new steady state,

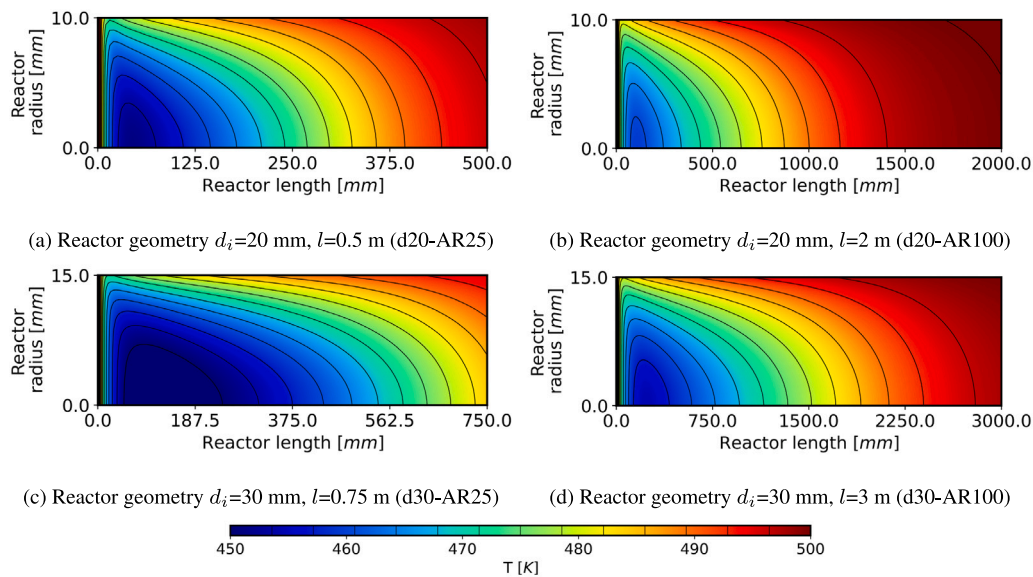


Fig. 5. Internal temperature fields of four reactor geometries with $W_{cat}F_{CH_3OH} = 200$, and $T_{wall}=501$ (steady state 1).

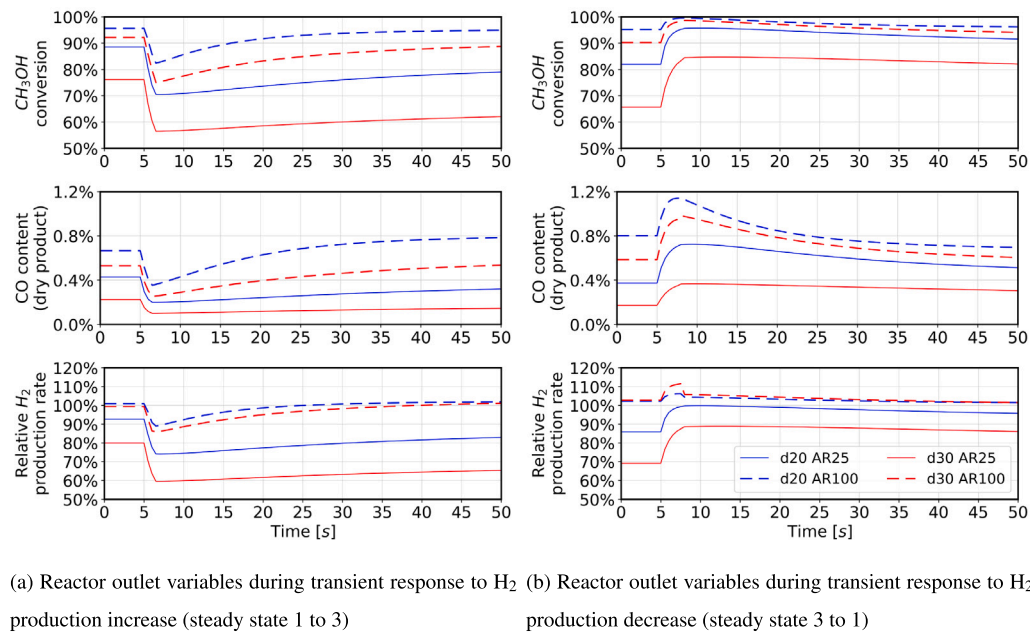


Fig. 6. Transient response of four simulated reactors geometries to step H_2 production increase by 100% from steady state 1 to 3, and step decrease from steady state 3 to 1.

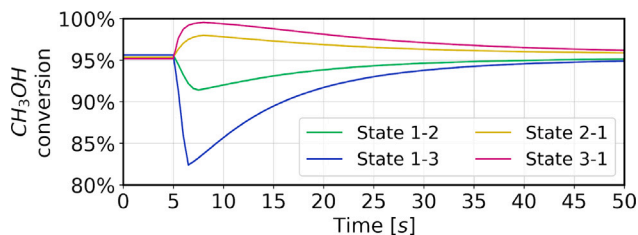


Fig. 7. Comparisons of CH_3OH conversions during step H_2 production increases by 50% and 100% (changing between states 1–2 and 1–3 respectively), and step returns to the original steady state 1 on reactor geometry $d_i=20$ mm and $l/d_i=100$ (d20-AR100).

since this metric indicates the time spent in inefficient operation due to low internal reactor temperature. In both AR25 and AR100 cases,

the diameter increase from 20 mm to 30 mm caused approximately 50% increase in conversion response. For AR increase four times on a constant diameter, the results show a decrease of 36% and 41% increase in response time for d20 and d30 reactors respectively. The reactor AR increase evidently had more influence in ramp up operation. In ramp downs, the reactors are compared with maximum increase of CO in the dry product, which is a consequence of temporary too high reactor temperature, and indicates a fluctuation of CO content that must be handled by the H_2 separation system. This comparison shows that diameter increase caused a relative maximum increase by 17% and 26% for AR25 and AR100 cases respectively. The reactor AR increase had a positive influence, since this metric decreased by 53% and 44% for d20 and d30 respectively. This comparison of geometric parameters on operation concludes different dominant influences for ramp up and ramp down procedures. Ultimately, the best performance is obtained by combining reactor length and small diameter, since the d20-AR100 reactor has the best performance by all metrics.

4.3. Discussion

The plotted performance metrics reveal a significant difference between increasing and decreasing the H₂ production. In ramp ups, the larger geometry and magnitude of H₂ demand change are correlated to disturbance size and transient time. Ramp up transients are sufficiently represented by the conversion plot. On the other hand, effects of ramp down events most negatively affect the CO production. Design of reactor and its inputs for forced operations should hence separately analyse production increasing and decreasing events for conversion drop and CO content increase respectively.

Maintaining CO levels of 0.2 ppm for low temperature PEMFC systems can be achieved in multiple ways. First, lower process temperature and pressure decrease CO selectivity. Second, the CO spike magnitude is proportional to throughput decrease. Decreasing the ramping rate reduces spikes in CO production. Third, the H₂ separation step can be designed for higher CO rates without drops in throughput and effectiveness [38,57]. For high temperature PEMFC, same strategies apply, except the CO tolerance is around 3%–5%, so the separator step can often be omitted [58,59]. The chosen combination of strategies may depend on the sought system design characteristics.

All simulated hydrogen production rates asymptotically approach the new value within one minute. This is comparable to the transient time of marine internal combustion engines [36,37], meaning catalyst thermal lag itself is not overly limiting. However, slower transients could be caused by the heat supply system. The reactor heating method, its control, and characteristic heat transfer resistance are thus highly influential to overall power system transient time. The system designer therefore must consider response time of heating system itself in addition to other characteristics discussed in Section 2.1, and decide on the best situation specific solution.

In commercial methanol reforming units, the stated hot stand by start up times in 5–45 min range [29,30,35] are presumably caused by the heating system transient time. Present off-the-shelf units heat the reactor by combustion of unpermeated gas from the membrane separation of H₂ [29,35], creating a complex system where the heating is dependent on reactor throughput and membrane permeation rate. This solutions prioritizes high autonomy and simple on-site installation, and thus opts for self-sustenance. If the heat is readily available from other sources, the reformer response could be improved most notably in start up operations.

4.3.1. Geometry and process variable limitations

Diameter choice influences the ratio between heated reactor wall area and internal catalyst volume. The ratio depends on the diameter according to:

$$\frac{A_{tube}}{V_{tube}} = \frac{C_{CS} l_{tube}}{A_{CS} l_{tube}} = \frac{\pi d_{tube}}{\pi (d_{tube}/2)^2} = \frac{4}{d_{tube}}, \quad (8)$$

where A_{tube} is the reactor tube area, V_{tube} is its volume, C_{CS} is the circumference of the tube cross section, A_{CS} is the area of the reactor tube cross section, l_{tube} is the reactor tube length, and d_{tube} is the reactor tube internal diameter. Increasing the diameter reduces available heating surface for the same volume of catalyst. The cases with d30 have generally lower conversion than d20, since using the same wall temperature across all cases means that d30 reactors received less heat per unit volume.

Equating the heat transfer rate in reactors with higher diameters could be realized by adjusting the wall temperature. However, different local maximum temperatures then influence process selectivity. Moreover, a higher wall temperature increases the cross section temperature gradient, causing differences in internal heat transfer rate. Every change in reactor geometry apparently influences process variables, so parametric studies of reactor dimensions are inherently not completely objective.

The uniform wall temperature simplification disregards the reactor tube heat capacity, and heat transfer from reactor filling to the tube. In

Table 5

Superficial fluid velocity and volumetric flow of reactants at the reactor inlet at steady state 1.

	d20 AR25	d20 AR100	d30 AR25	d30 AR100
u_s [m s ⁻¹]	7.08e-2	28.35e-2	10.71e-2	42.84e-2
Q [m ³ s ⁻¹]	2.22e-5	8.9e-5	7.57e-5	30.28e-5

reality, the tube also needs time to heat up, slowing down the ramp up operations. In ramp downs, the residual heat in the tube could potentially cause higher or longer CO spikes since it keeps heating the reactor for longer. However, in reality the tube heat can also be transferred back to the heating fluid so the extent of this issue in ramp down is hard to assume. This problem requires more detailed modelling with defined and simulated heating method.

The simulations show that flow velocity affects the radial heat distribution, but it is not the most determining factor. Higher superficial fluid velocities are observed in d30 reactors than the d20 counterparts, summarized in Table 5, but the heat distribution is worse according to the steady state temperature plots. A larger reactor diameter counteracts the benefits from higher fluid velocity for multiple reasons. First, the heat has to penetrate deeper into the reactor. Second, there is less heating area at larger diameters, as discussed previously. Similarly, larger diameters have higher volumetric flow Q , as seen in Table 5, further implying a larger heating requirement. Overall the results indicate that increased reactor diameters require higher flow velocities and aspect ratios to maintain selectivity and transient response time.

5. Conclusions

The present work focuses on transient states of methanol steam reformers and offers novel insight into dominant influences on internal flow fields, heat transfer, and overall performance during H₂ demand changes. The effects of different geometries of reactor tubes and process variables in unsteady state are analysed through numerical modelling. Key points for methanol steam reformers in the analysed range of dimensions from the current study are:

1. The transient time of the reformer tube and H₂ production stabilization is around 30 s in most cases,
2. Good selectivity and temperature distribution from small diameters and high aspect ratios also provide faster response and lower conversion drop in transients,
3. Transient time in ramp ups is influenced by reactor geometry and change magnitude much more than transients in ramp downs,
4. CH₃OH conversion is the most important performance metric in ramp up operations, while CO content in the product is the most important in ramp downs,
5. Aspect ratio is a more objective metric than length, but not completely independent from diameter,
6. Duration of transients in practice is likely predominantly dependent on reactor heat supply.

Following the present work, experimental validation of the dynamic part of the model is required. In addition, further dynamic simulations including a specific heating method effects are required. The present study is limited with uniform wall temperature assumption, so inclusion of realistic heating systems is required for capturing their effects on the internal heat transfer and reaction rates, which are difficult to study experimentally. Simulations with broader geometry and process variable parameter space are also recommended for better generalization of the results. Furthermore, the choice of a heating method is a closely related subject of interest. The choice may be influenced by

performances of each method, but also depends on the technical and economical constraints of the heating system in an environment such as maritime. The heating system might also have to integrate with other on board systems and processes, steering the analysis towards an entire system design.

This work is performed in the interest of better integration of methanol steam reformers into maritime setting. At present, the only option for on-board H_2 production from methanol is via autonomous commercial reforming systems. Despite their convenience, integrating the reformer with other on-board waste heat systems could be increase efficiency, compactness, and transient response time. Furthermore, potential carbon capturing is also possible and integrating it directly into the methanol conversion process allows capturing a relatively pure stream of CO_2 . This study shows that dynamic operation of methanol reformers, as well as the entire methanol based fuel cell system, is not highly dependent on stabilization of reformer H_2 production, but rather mostly depends on heat integration and control strategy of the system. If slower unsteady operation is compulsory due to the heating system, quickly filling the H_2 demand will be a larger issue than spikes in CO production. Transient modelling studies for system design should be hence addressed by including the reactor heating method, or with prior knowledge of its limitation in unsteady operation.

Efficient usage of methanol and easy opportunities for carbon capture simultaneously promote a circular methanol cycle, and help control harmful airborne emissions. Preserving this efficiency in unsteady operation is paramount for transport applications, to which this study contributes. The urgent maritime emission requirements and wide array of system sizes in the shipping industry provide great examples for methanol reforming systems in many other fields faced with restrictive emission standards.

CRedit authorship contribution statement

Bojan Grenko: Writing – original draft, Visualization, Validation, Software, Methodology, Investigation, Data curation, Conceptualization. **Wiebren de Jong:** Writing – review & editing, Supervision, Conceptualization. **Robert van de Ketterij:** Writing – review & editing, Supervision, Conceptualization. **Lindert van Biert:** Writing – review & editing, Supervision, Funding acquisition, Conceptualization.

Declaration of competing interest

The authors declare that they have no known competing financial interests or personal relationships that could have appeared to influence the work reported in this paper.

Acknowledgements

Present work is part of the MENENS (Methanol als Energiestap Naar Emissieloze Nederlandse Scheepvaart) project. The project is funded by the Netherlands Enterprise Agency (RVO: Rijksdienst voor Ondernemend Nederland) under the grant number MOB21012.

Appendix A. Supplementary data

Supplementary material related to this article can be found online at <https://doi.org/10.1016/j.ccej.2025.160623>.

Data availability

Data will be made available on request.

References

- [1] Official Journal of the European Union, L 243, 9 July 2021, Official Journal L 243/1 (2021) 1–51, URL <https://eur-lex.europa.eu/legal-content/EN/TXT/?uri=OJ:L:2021:243:TOC>.
- [2] International Maritime Organisation, MARPOL Consolidated edition 2017, Sixth ed., International Maritime Organisation, 2017, ISBN:9789280116571.
- [3] Paris agreement, 2015, URL https://treaties.un.org/pages/ViewDetails.aspx?src=TREATY&mtdsg_no=XXVII-7-d&chapter=27&clang=en.
- [4] L. van Biert, M. Godjevac, K. Visser, P. Aravind, A review of fuel cell systems for maritime applications, *J. Power Sources* 327 (2016) 345–364, <http://dx.doi.org/10.1016/j.jpowsour.2016.07.007>, URL <https://www.sciencedirect.com/science/article/pii/S0378775316308631>.
- [5] A.G. Elkafas, M. Rivarolo, E. Gadducci, L. Magistri, A.F. Massardo, Fuel cell systems for maritime: A review of research development, commercial products, applications, and perspectives, *Processes* 11 (1) (2023) <http://dx.doi.org/10.3390/pr11010097>, URL <https://www.mdpi.com/2227-9717/11/1/97>.
- [6] R.G.v.d. Ketterij, R. Geertsma, A. Grasman, M. Pothaar, A. Coraddu, Alternative fuels, propulsion and power systems for the future navy – a route towards reduced emissions and signatures, and fossil fuel independence, in: G. Frerks, R. Geertsma, J. Klomp, T. Middendorp (Eds.), *Climate Security and the Military: Concepts, Strategies, and Partnerships*, in: LUP NL ARMS, vol. 2023, Leiden University Press, 2024, <http://dx.doi.org/10.24415/9789400604780-019>.
- [7] K. Hyde, A. Ellis, I. Power, Feasibility of hydrogen bunkering, ITM Power (2019) URL <https://northsearegion.eu/media/9385/feasibility-of-hydrogen-bunkering-final-080419.pdf>.
- [8] European Maritime Safety Agency, Potential of hydrogen as fuel for shipping, EMSA (2023) URL <https://emsa.europa.eu/publications/reports/item/5062-potential-of-hydrogen-as-fuel-for-shipping.html>.
- [9] Methanol Institute, Marine methanol: Future-proof shipping fuel, Methanol Institute (2023) URL https://www.methanol.org/wp-content/uploads/2023/05/Marine_Methanol_Report_Methanol_Institute_May_2023.pdf.
- [10] A. Forsyth, All at sea - methanol and shipping, Longspur Research (2022) URL <https://www.methanol.org/wp-content/uploads/2022/01/Methanol-and-Shipping-Longspur-Research-25-Jan-2022.pdf>.
- [11] A.M. Ranjekar, G.D. Yadav, Steam reforming of methanol for hydrogen production: A critical analysis of catalysis, processes, and scope, *Ind. Eng. Chem. Res.* 60 (2021) 89–113, <http://dx.doi.org/10.1021/acs.iecr.0c05041>, URL <https://pubs.acs.org/doi/10.1021/acs.iecr.0c05041>.
- [12] K. Kappis, J. Papavasiliou, G. Avgouropoulos, Methanol reforming processes for fuel cell applications, *Energies* 14 (2021) 8442, <http://dx.doi.org/10.3390/EN14248442>, <https://www.mdpi.com/1996-1073/14/24/8442/htm>, <https://www.mdpi.com/1996-1073/14/24/8442>.
- [13] IRENA and Methanol Institute, Innovation Outlook: Renewable Methanol, International Renewable Energy Agency, 2021, URL https://www.methanol.org/wp-content/uploads/2020/04/IRENA_Innovation_Renewable_Methanol_2021.pdf.
- [14] Hydrogen One towboat, URL <https://www.ebdg.com/hydrogenone>, Accessed: 2025-01-06.
- [15] K.F. Kalz, R. Kraehnert, M. Dvoyashkin, R. Dittmeyer, R. Gläser, U. Krewer, K. Reuter, J.-D. Grunwaldt, Future challenges in heterogeneous catalysis: Understanding catalysts under dynamic reaction conditions, *ChemCatChem* 9 (1) (2017) 17–29, <http://dx.doi.org/10.1002/cctc.201600996>, URL <https://chemistry-europe.onlinelibrary.wiley.com/doi/abs/10.1002/cctc.201600996>.
- [16] Z. Hua, Z. Zheng, E. Pahan, M.-C. Péra, F. Gao, Remaining useful life prediction of PEMFC systems under dynamic operating conditions, *Energy Convers. Manage.* 231 (2021) 113825, <http://dx.doi.org/10.1016/j.enconman.2021.113825>, URL <https://www.sciencedirect.com/science/article/pii/S0196890421000029>.
- [17] Nedstack Fuel Cell Technology, PemGen CHP-FCPS-120, URL <https://nedstack.com/en/pemgen-solutions/stationary-fuel-cell-power-systems/pemgen-chp-fcps-120>, Accessed: 2024-08-12.
- [18] Ballard Power Systems, FCgen-HPS, URL https://www.ballard.com/about-ballard/publication_library/product-specification-sheets/fcgen-hps-spec-sheet, Accessed: 2024-08-12.
- [19] Proton Motor Hydrogen Fuel Cells, MyModule Fuel Cell, URL <https://www.proton-motor.com/en/hymodule/>, Accessed: 2024-08-12.
- [20] G. Bernardo, T. Araújo, T. da Silva Lopes, J. Sousa, A. Mendes, Recent advances in membrane technologies for hydrogen purification, *Int. J. Hydrog. Energy* 45 (12) (2020) 7313–7338, <http://dx.doi.org/10.1016/j.ijhydene.2019.06.162>, URL <https://www.sciencedirect.com/science/article/pii/S0360319919324620>, Hydrogen separation/purification via membrane technology.
- [21] Element 1, Element1 Hydrogen Purifier, URL <https://www.e1na.com/hydrogen-purifier-module>, Accessed: 2024-08-13.
- [22] M. Amin, A.S. Butt, J. Ahmad, C. Lee, S.U. Azam, H.A. Mannan, A.B. Naveed, Z.U.R. Farooqi, E. Chung, A. Iqbal, Issues and challenges in hydrogen separation technologies, *Energy Rep.* 9 (2023) 894–911, <http://dx.doi.org/10.1016/j.egy.2022.12.014>, URL <https://linkinghub.elsevier.com/retrieve/pii/S2352484722026130>.

- [23] A. Lotrič, M. Sekavčnik, S. Hočevar, Effectiveness of heat-integrated methanol steam reformer and polymer electrolyte membrane fuel cell stack systems for portable applications, *J. Power Sources* 270 (2014) 166–182, <http://dx.doi.org/10.1016/j.jpowsour.2014.07.072>, URL <https://www.sciencedirect.com/science/article/pii/S0378775314011161>.
- [24] Y. Wang, Q. Wu, D. Mei, Y. Wang, Development of highly efficient methanol steam reforming system for hydrogen production and supply for a low temperature proton exchange membrane fuel cell, *Int. J. Hydrog. Energy* 45 (46) (2020) 25317–25327, <http://dx.doi.org/10.1016/j.ijhydene.2020.06.285>, URL <https://www.sciencedirect.com/science/article/pii/S0360319920324952>.
- [25] D. Yu, N.T. Van, J. Yun, S. Yu, a thermal design of a 1 kW-Class shell and tube methanol steam reforming system with internal evaporator, *Processes* 8 (2020) 1509, <http://dx.doi.org/10.3390/PR8111509>, <https://www.mdpi.com/2227-9717/8/11/1509/htm>, <https://www.mdpi.com/2227-9717/8/11/1509>.
- [26] P. Ribeirinha, M. Abdollahzadeh, J.M. Sousa, M. Boaventura, A. Mendes, Modelling of a high-temperature polymer electrolyte membrane fuel cell integrated with a methanol steam reformer cell, *Appl. Energy* 202 (2017) 6–19, <http://dx.doi.org/10.1016/J.APENERGY.2017.05.120>.
- [27] N. Li, X. Cui, J. Zhu, M. Zhou, V. Liso, G. Cinti, S.L. Sahlin, S.S. Araya, A review of reformed methanol-high temperature proton exchange membrane fuel cell systems, *Renew. Sustain. Energy Rev.* 182 (2023) 113395, <http://dx.doi.org/10.1016/j.rser.2023.113395>, URL <https://www.sciencedirect.com/science/article/pii/S1364032123002526>.
- [28] G. Garcia, E. Arriola, W.H. Chen, M.D.D. Luna, A comprehensive review of hydrogen production from methanol thermochemical conversion for sustainability, *Energy* 217 (2021) 119384, <http://dx.doi.org/10.1016/J.ENERGY.2020.119384>.
- [29] RIX Industries, M2H2 Series Mobile Hydrogen Generator, URL <https://www.rixindustries.com/hydrogen-generation-systems>, Accessed: 2024-08-05.
- [30] MMM Energy, M Reformer Hydrogen Generator, URL <https://www.methanolreformer.com/>, Accessed: 2024-08-05.
- [31] M. Rostami, A.H. Farajollahi, R. Amirkhani, M.E. Farshchi, A review study on methanol steam reforming catalysts: Evaluation of the catalytic performance, characterizations, and operational parameters, *AIP Adv.* 13 (3) (2023) 030701, <http://dx.doi.org/10.1063/5.0137706>.
- [32] Z. Huang, J. Shen, S.H. Chan, Z. Tu, Transient response of performance in a proton exchange membrane fuel cell under dynamic loading, *Energy Convers. Manage.* 226 (2020) 113492, <http://dx.doi.org/10.1016/j.enconman.2020.113492>, URL <https://www.sciencedirect.com/science/article/pii/S0196890420310244>.
- [33] Q. Yang, B. Gao, G. Xiao, D. Jin, Analysis of PEMFC undershoot behavior and performance stabilization under transient loading, *Int. J. Hydrog. Energy* 50 (2024) 1358–1372, <http://dx.doi.org/10.1016/j.ijhydene.2023.07.013>, URL <https://www.sciencedirect.com/science/article/pii/S0360319923033839>.
- [34] C.-H. Lee, J.-T. Yang, Modeling of the ballard-mark-v proton exchange membrane fuel cell with power converters for applications in autonomous underwater vehicles, *J. Power Sources* 196 (8) (2011) 3810–3823, <http://dx.doi.org/10.1016/j.jpowsour.2010.12.049>, URL <https://www.sciencedirect.com/science/article/pii/S037877531002255X>.
- [35] S-Series Hydrogen Generator, URL <https://www.e1na.com/s-series-hydrogen-generator>, Accessed: 2024-08-13.
- [36] Wartsila Corporation, Combustion engine vs. Aeroderivative gas turbine: Six elements of dispatching, URL <https://www.wartsila.com/energy/learn-more/technology-comparison-engines-vs-aeros/six-elements-of-dispatching>, Accessed: 2024-09-18.
- [37] MAN Energy Solutions, MAN 175D: Four-stroke high-speed diesel engine compliant with IMO Tier II / IMO Tier III, Tech. rep., MAN Energy Solutions, 2024, URL https://man-es.com/applications/projectguides/4stroke/Propulsion/PG_P-II_175D.pdf.
- [38] F. Pinto, R.N. André, C. Franco, C. Carolino, I. Gulyurtlu, Effect of syngas composition on hydrogen permeation through a Pd–Ag membrane, *Fuel* 103 (2013) 444–453, <http://dx.doi.org/10.1016/j.fuel.2012.05.060>, URL <https://linkinghub.elsevier.com/retrieve/pii/S0016236112004176>.
- [39] A.B. Leyko, A.K. Gupta, Temperature and pressure effects on hydrogen separation from syngas, *J. Energy Resour. Technol.* 135 (3) (2013) 034502, <http://dx.doi.org/10.1115/1.4024028>.
- [40] G. Towler, R. Sinnott, Chapter 19 - heat transfer equipment, in: G. Towler, R. Sinnott (Eds.), *Chemical Engineering Design*, third ed., Butterworth-Heinemann, 2022, pp. 823–951, <http://dx.doi.org/10.1016/B978-0-12-821179-3.00019-4>, URL <https://www.sciencedirect.com/science/article/pii/B9780128211793000194>.
- [41] G. Eigenberger, W. Ruppel, Catalytic fixed-bed reactors, in: *Ullmann's Encyclopedia of Industrial Chemistry*, John Wiley & Sons, Ltd, 2012, http://dx.doi.org/10.1002/14356007.b04_199.pub2.
- [42] Y.T. Kim, J.-J. Lee, J. Lee, Electricity-driven reactors that promote thermochemical catalytic reactions via joule and induction heating, *Chem. Eng. J.* 470 (2023) 144333, <http://dx.doi.org/10.1016/j.cej.2023.144333>, URL <https://www.sciencedirect.com/science/article/pii/S1385894723030644>.
- [43] M. Idamakanti, E.B. Ledesma, R.R. Ratnakar, M.P. Harold, V. Balakotaiah, P. Bollini, Electrified catalysts for endothermic chemical processes: Materials needs, advances, and challenges, *ACS Eng. Au* 4 (1) (2024) 71–90, <http://dx.doi.org/10.1021/acsengineeringau.3c00051>.
- [44] J. Zhu, S.S. Araya, X. Cui, S.L. Sahlin, S.K. Kær, Modeling and design of a multi-tubular packed-bed reactor for methanol steam reforming over a Cu/ZnO/Al₂O₃ catalyst, *Energies* 13 (3) (2020) <http://dx.doi.org/10.3390/en13030610>, URL <https://www.mdpi.com/1996-1073/13/3/610>.
- [45] J. Zhu, X. Cui, S.S. Araya, Comparison between 1D and 2D numerical models of a multi-tubular packed-bed reactor for methanol steam reforming, *Int. J. Hydrog. Energy* 47 (54) (2022) 22704–22719, <http://dx.doi.org/10.1016/j.ijhydene.2022.05.109>, URL <https://www.sciencedirect.com/science/article/pii/S0360319922021474>.
- [46] A. Sari, J. Sabziani, Modeling and 3D-simulation of hydrogen production via methanol steam reforming in copper-coated channels of a mini reformer, *J. Power Sources* 352 (2017) 64–76, <http://dx.doi.org/10.1016/j.jpowsour.2017.03.120>, URL <https://linkinghub.elsevier.com/retrieve/pii/S0378775317304342>.
- [47] O. Klenov, L. Makarshin, A. Gribovskiy, D. Andreev, V. Parmon, CFD modeling of compact methanol reformer, *Chem. Eng. J.* 282 (2015) 91–100, <http://dx.doi.org/10.1016/j.cej.2015.04.006>, URL <https://linkinghub.elsevier.com/retrieve/pii/S1385894715004817>.
- [48] H.S. Fogler, *Elements of Chemical Reaction Engineering*, fourth ed., Prentice Hall, 2005.
- [49] B.A. Peppley, J.C. Amphlett, L.M. Kearns, R.F. Mann, Methanol-steam reforming on Cu/ZnO/Al₂O₃ catalysts. Part 2. A comprehensive kinetic model, *Appl. Catal. A: General* 179 (1999) 31–49, [http://dx.doi.org/10.1016/S0926-860X\(98\)00299-3](http://dx.doi.org/10.1016/S0926-860X(98)00299-3).
- [50] J. Zhu, Modelling of a packed-bed methanol steam reformer for HT-PEM fuel cell applications, in: Ph.D.-serien for Det Ingeniør- og Naturvidenskabelige Fakultet, Aalborg Universitet, Aalborg Universitetsforlag, 2022, <http://dx.doi.org/10.54337/auu513444640>.
- [51] H.C. Yoon, J. Otero, P.A. Erickson, Reactor design limitations for the steam reforming of methanol, *Appl. Catal. B: Environ.* 75 (2007) 264–271, <http://dx.doi.org/10.1016/j.apcatb.2007.04.017>, URL <https://linkinghub.elsevier.com/retrieve/pii/S0926337307001257>.
- [52] B. Grenko, Dynamic 2D methanol reformer, 2024, <http://dx.doi.org/10.5281/zenodo.13736015>.
- [53] C. Pan, R. He, Q. Li, J.O. Jensen, N.J. Bjerrum, H.A. Hjulmand, A.B. Jensen, Integration of high temperature PEM fuel cells with a methanol reformer, *J. Power Sources* 145 (2005) 392–398, <http://dx.doi.org/10.1016/j.jpowsour.2005.02.056>, URL <https://linkinghub.elsevier.com/retrieve/pii/S0378775305002752>.
- [54] A. Chougule, R.R. Sonde, Modelling and experimental investigation of compact packed bed design of methanol steam reformer, *Int. J. Hydrog. Energy* 44 (2019) 29937–29945, <http://dx.doi.org/10.1016/j.ijhydene.2019.09.166>, URL <https://linkinghub.elsevier.com/retrieve/pii/S036031991933589X>.
- [55] R. Peters, H. Düsterwald, B. Höhle, Investigation of a methanol reformer concept considering the particular impact of dynamics and long-term stability for use in a fuel-cell-powered passenger car, *J. Power Sources* 86 (2000) 507–514, [http://dx.doi.org/10.1016/S0378-7753\(99\)00477-2](http://dx.doi.org/10.1016/S0378-7753(99)00477-2), URL <https://linkinghub.elsevier.com/retrieve/pii/S0378775399004772>.
- [56] C. Agrafiotis, H. von Storch, M. Roeb, C. Sattler, Solar thermal reforming of methane feedstocks for hydrogen and syngas production—A review, *Renew. Sustain. Energy Rev.* 29 (2014) 656–682, <http://dx.doi.org/10.1016/j.rser.2013.08.050>, URL <https://www.sciencedirect.com/science/article/pii/S136403211300590X>.
- [57] N. Zhang, J. Xiao, P. Bénard, R. Chahine, Single- and double-bed pressure swing adsorption processes for H₂/CO syngas separation, *Int. J. Hydrog. Energy* 44 (48) (2019) 26405–26418, <http://dx.doi.org/10.1016/j.ijhydene.2019.08.095>, URL <https://www.sciencedirect.com/science/article/pii/S036031991933068X>.
- [58] J. Zhang, C. Zhang, J. Li, B. Deng, M. Fan, M. Ni, Z. Mao, H. Yuan, Multi-perspective analysis of CO poisoning in high-temperature proton exchange membrane fuel cell stack via numerical investigation, *Renew. Energy* 180 (2021) 313–328, <http://dx.doi.org/10.1016/j.renene.2021.08.089>, URL <https://www.sciencedirect.com/science/article/pii/S096014812101257X>.
- [59] Y. Devrim, A. Albostan, H. Devrim, Experimental investigation of CO tolerance in high temperature PEM fuel cells, *Int. J. Hydrog. Energy* 43 (40) (2018) 18672–18681, <http://dx.doi.org/10.1016/j.ijhydene.2018.05.085>, URL <https://www.sciencedirect.com/science/article/pii/S036031991831601X>.